Cross sections for the Ti(p,n) reaction to analogs of ground and 2^+ excited states

V. R. Brown, C. Wong, C. H. Poppe, J. D. Anderson, and J. C. Davis
Lawrence Livermore National Laboratory, Livermore, California 94550

S. M. Grimes
Lawrence Livermore National Laboratory, Livermore, California 94550
and Department of Physics, Ohio University, Athens, Ohio 45701

V. A. Madsen
Lawrence Livermore National Laboratory, Livermore, California 94550
and Department of Physics, Oregon State University, Corvallis, Oregon 97331
(Received 8 July 1985)

Cross sections for the (p,n) reaction to analog states have been measured for the five stable isotopes of titanium at energies between 11.5 and 26 MeV. In addition to the ground-state analogs, cross sections to the 2_1^+ analog states for the even A isotopes have been determined. A two-channel analysis of the ground-state analog data, searching on the charge-exchange parameters, did not yield a satisfactory globally consistent description of the 0_1^+ analog cross sections. However, in a full coupled-channel description of the 0_1^+ analog angular distributions the $N-Z$ dependence and the strength of the 2_1^+ analog cross sections for ^{46,48,50}Ti are explained by strong inelastic couplings and by rather different charge-exchange couplings among the three isotopes. The isovector deformation parameters used in the charge-exchange couplings were determined from electromagnetic and (p,p') values, which were obtained from experiment. The experimental energy dependence of the cross section shows a resonance behavior which is not explained by the channel coupling but which can be adequately accounted for by an energy dependent V_1.

I. INTRODUCTION

The (p,n) reaction populating the analog of the target ground state at energies less than 50 MeV is usually interpreted with the Lane model.[1] It is postulated that both the real and imaginary components of the nucleon optical potential have a term proportional to the inner product of the isospins of target and projectile; this term can induce charge-exchange transitions, resulting in (p,n) reactions populating the analog of the target ground state. The Lane model predicts cross sections and angular distributions which are in reasonably good agreement with (p,n) data.

Some anomalies[2-6] have been found for targets for which cross sections have been measured at many energies. The optical potential parameters obtained for elastic scattering of protons and neutrons suggest that the energy dependence of the isospin-dependent term is smooth, while analog cross sections often show a resonant behavior, which can be reproduced only with an energy dependent strength in the isospin potential.

In the study of Miller and Garvey[2] the cross sections were measured near threshold; these authors concluded that the modulation in cross section was due to the energy dependence of the imaginary potential for low energy neutrons. For other cases, for example the Mo isotopes,[7] resonant behavior occurs above threshold, and is therefore less likely to be due to the energy dependence of the optical potential.

Measurements[7-10] of the cross sections on neighboring isotopes show that ground-state analog cross sections are not linearly proportional to $(N-Z)$, as would be expected from the Lane model in the distorted-wave Born approximation (DWBA). The odd isotopes have a larger cross section than the even ones, and in addition the even isotopes have shown systematic departures from constancy of $\sigma/(N-Z)$. It has been shown[9-11] that at a given incident energy collective-coupling effects can explain the nonlinear dependence on neutron excess of the even isotopes, but this coupling does not appear to be responsible for the rapid energy dependence. The present measurements were undertaken to determine the energy dependence of the cross section and to see whether the $N-Z$ anomaly seen in other nuclei is also present in the Ti isotopes. Data taken for the odd isotopes ^{47}Ti and ^{49}Ti are also presented but the theoretical analysis is limited to the even nuclei.

In Sec. II the experimental method is described. In Sec. III, results of an analysis of the (p,n) reaction in terms of the Lane model are given, in which only the coupling of the target ground state and its analog in the residual nucleus is included. Lane-potential parameters V_1 and W_1 are obtained by searches on the (p,n) analog data, holding the proton optical potential parameters fixed. Section IV contains results of a coupled-channel analysis in which the ground state, the 2_1^+ state, the $0_2^+,2_2^+,4_1^+$ triplet, and their analogs are included. The empirical differences of deformation parameters, $\beta_n \neq \beta_p$, in the 2_1^+ nuclear vibration and the effects of the implied isovector deformation parameter β_1 on the (p,n) charge-exchange reaction are

presented. Section V contains our summary and discussion.

II. EXPERIMENTAL METHOD

Cross sections for the (p,n) reaction to the ground-state and excited-state analogs for the five stable titanium isotopes were measured with the multidetector time-of-flight spectrometer at the Lawrence Livermore National Laboratory. Measurements at proton energies of 12 MeV or less were made with the beam of the EN tandem accelerator, while those at higher energies utilized the cyclograaff facility (a 15 MeV cyclotron coupled to the tandem accelerator).

NE 213 scintillators served as neutron detectors; the pulse shape discrimination properties of this scintillator were exploited to reduce the background caused by gamma-ray-induced pulses. Neutron energies were inferred from the measurements of the flight time over a 10.8 m flight path.

Self-supporting targets of thickness about 4 mg/cm^2 were obtained from the Isotopes Division of Oak Ridge National Laboratory. The enrichments were 81.2%, 80.1%, 99.1%, 81.6%, and 76.4% for the isotopes 46—50, respectively. At bombarding energies below 12 MeV, the neutron energy resolution was sufficiently good so as to allow the separation of the contribution of the ^{48}Ti impurity from the analog cross sections of the heavier Ti isotopes (a peak corresponding to the analog state transition in ^{48}Ti was found for the targets of the ^{49}Ti and ^{50}Ti isotopes); above this energy, the contribution from the other isotopes was subtracted out for each target, based on known abundances and the measured cross sections.

A typical spectrum at 24 MeV (Ref. 12) is shown in Fig. 1. At low energies numerous peaks were seen in the spectra, but for energies above 17 MeV only peaks corresponding to analogs of the ground state and (for even targets) the 2_1^+ state were seen. Although analogs of excited states in ^{49}Ti could have been resolved at all energies, they were detected only for energies below 15 MeV. The analog of the first excited state of ^{47}Ti is sufficiently close to the ground-state analog that it could not be resolved at higher energies, but no correction was applied since the corresponding state in ^{49}Ti was so weakly populated.

Each of the angular distributions was fitted with a series of Legendre polynomials in order to determine the integrated cross section. Errors in the integrated cross sections were determined from both the relative errors in the individual points and from the goodness of fit of the polynomial representation of the data. At forward angles the largest contribution to the error on the individual point was due to uncertainty in the background subtraction while at large angles the statistical errors dominated. The uncertainties due to the polynomial fits were generally less than 5%. The overall errors on the integrated cross sections were estimated to be ~10%. However, extraction of cross sections was more difficult than in the Mo isotopes because of the presence of nonanalog discrete states, so these error estimates may be optimistic. Figure 2 shows the differential cross sections for the ^{47}Ti(p,n)^{47}V and ^{49}Ti(p,n)^{49}V to ground-state analogs at 15.3 and 26

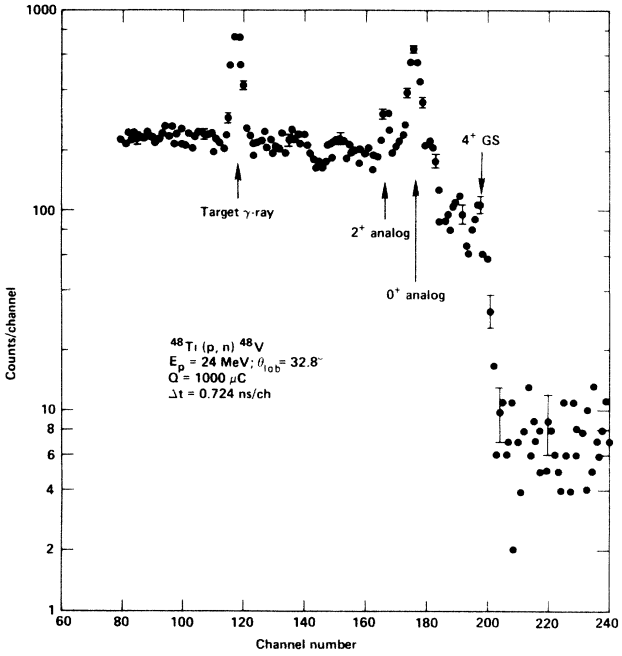

FIG. 1. The (p,n) spectrum for the ^{48}Ti(p,n)^{48}V reaction at a proton energy of 24 MeV at an angle of 32.8°. The arrows indicate neutrons emitted upon populating the 0_1^+ and 2_1^+ analogs and the ground state of ^{48}V.

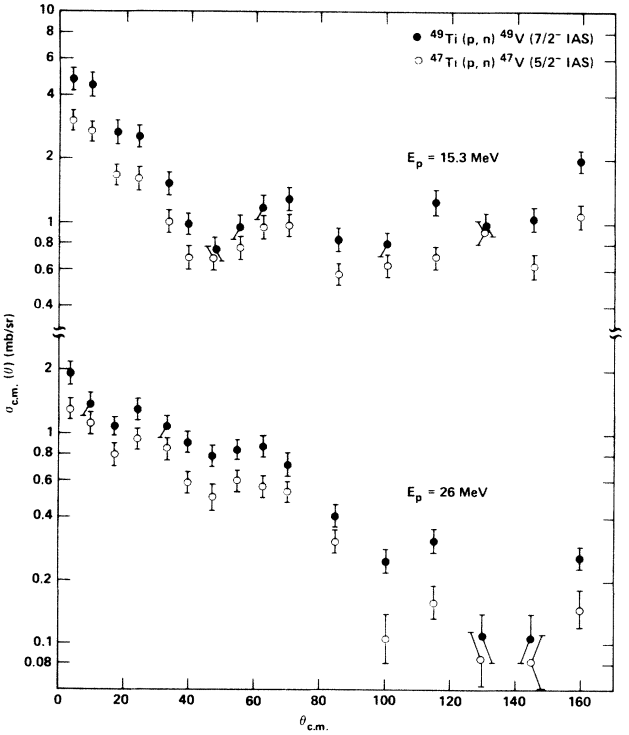

FIG. 2. Angular distribution for the ^{47}Ti(p,n)^{47}V and ^{49}Ti(p,n)^{49}V reactions to the ground-state analogs at 15.3 and 26 MeV.

TABLE I. Integrated analog cross sections. The overall errors on the integrated cross sections were estimated to be ~10%.

	0_1^+ (mb)				
E (MeV)/A	46	47	48	49	50
11.5	6.2	7.3	8.5	15.6	26.3
15.3	4.9	10.7	8.6	15.4	18.0
17	3.5	5.9	8.0	12.1	13.0
22	1.9	5.7	5.9	8.0	6.3
26	1.4	4.4	4.9	6.4	5.2

	2_1^+ (mb)		
E (MeV)/A	46	48	50
11.5	6.8	1.2	
15.3	3.3	3.0	1.9
17	1.9	2.3	2.5
22	1.3	0.93	0.74
26	0.94	0.7	0.61

MeV. Corresponding results for the even isotopes are shown in Sec. IV. Table I and Fig. 3 show the integrated cross sections for all isotopes.

The energy dependence of the cross sections is reasonably smooth but does vary somewhat among the various isotopes. A much more rapid falloff with increasing energy occurs for ^{46}Ti and for ^{50}Ti than for ^{48}Ti. The odd isotopes show a generally less rapid energy dependence than the even isotopes.

III. TWO-CHANNEL ANALYSIS AND SEARCHES

The cross sections for the (p,n) reaction to the isobaric analog of the target ground state below 50 MeV are normally calculated with the Lane equations. These are based on the presence of a term depending on the product $t \cdot T$ in the optical potential. This term is capable both of modifying the potential for elastic scattering of protons relative to that for neutrons and of inducing the transition between the proton-plus-target and neutron-plus-analog channels.

Angular distributions for the (p,n) reaction to the analog state were first fit with isovector potentials without including any other states. Separate fits were performed with the geometries and potential strengths given by Becchetti and Greenlees[13] (BG) and by Rosen *et al.*[14] In each case the isovector potential was assumed to have a real and an imaginary component, each of which was given the geometry of the corresponding isoscalar part. In both searches, the neutron potential was determined so as to be consistent with isospin conservation, i.e., the isoscalar and isovector terms were set equal to those for protons with the sign modified for the isovector. The fitting procedure consisted of varying the real and imaginary isovector strengths so as to minimize deviations between calculated and measured angular distributions. These results were used as a starting point for the coupled channels analysis in Sec. IV A.

Seeking an explanation for the energy dependence found[7] in the analog cross sections of the molybdenum isotopes, the authors of Ref. 7 considered the possibility that single-particle resonances were the source of the energy dependence. Strictly, such effects should be incorporated in direct-reaction calculations automatically, but, if the optical potential parameters were not correct, it could be argued that a single-particle resonance might be moved to an incorrect energy. The calculation presented in Ref. 8 also indicated, however, that the imaginary po-

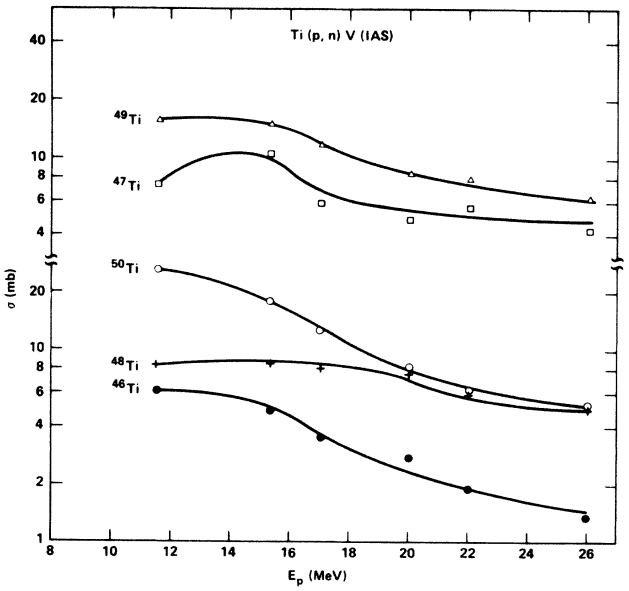

FIG. 3. Angle-integrated cross sections for population of ground-state analogs with the (p,n) reaction on targets of $^{46-50}$Ti. The lines are simply guides to the eye.

tential parameters, in general use, implied a substantial damping of the single-particle states, with the result that the single-particle states are spread over many MeV. This would be expected to smooth out the energy dependence of the cross section to the point that no resonances would be seen. The possibility remains that a complicated l-dependent imaginary potential might have sufficiently weak absorption in a particular angular momentum channel that a single-particle resonance could remain narrow.

The energy dependence of the present data, though more rapid than expected from analysis of data at higher energies, does not show 3—4 MeV wide peaks as was seen for Mo. An enhancement in the surface (imaginary) component was found in the 17 MeV region with the potential of Ref. 13; interestingly, the corresponding search with the potential of Patterson *et al.*[15] did not yield such an enhancement. In both cases, however, the cross section arises largely from contributions from $l=3$ and 4 channels in this energy region.

Single-particle resonances were found for the optical potentials of Wilmore and Hodgson,[16] Ref. 14, and Ref. 13 as well as the neutron potential of Ref. 14. As was found[7] for the Mo isotopes, the imaginary potential used in optical potentials broadens the single-particle states to make them many MeV wide. By reducing the imaginary potential strength to 1 MeV and calculating the absorption cross section, it was possible to produce narrow resonances in some angular momentum channels. For both protons and neutrons the resonances are found in the $l=2$, 4, and 5 channels. These are the $d_{5/2}$, $g_{7/2}$, and $h_{11/2}$ states of higher oscillator shells. Even with a very small value for W, some single-particle states do not show up as narrow resonances in the optical-model calculations. Shell-model calculations would suggest that an $s_{1/2}$ and a $d_{3/2}$ state should be in the experimental energy region, but the calculations show no resonances in these channels. If the state is too far above the angular momentum barrier (plus Coulomb barrier for protons), it will not become narrow even when W is reduced. The proton single-particle states are displaced by the Coulomb energy from the neutron states, but, because of the presence of the Coulomb barrier, they are roughly as narrow for protons as for neutrons. Moreover, this displacement causes the two sets of resonances (proton and neutron) to occur at the same compound system energy for a (p,n) reaction to the analog state. Thus, resonance effects would probably be seen in both entrance and exit channels if they are present in one.

Some variation in single-particle energy is observed when comparing the various optical-model calculations. The $d_{5/2}$ state was near 3 MeV in the neutron channel but did vary more than 1 MeV between the Becchetti and Greenlees[13] and the Wilmore and Hodgson potential,[16] with that of Rosen *et al.*[14] in between. Similarly, the $g_{7/2}$ and $h_{11/2}$ states were found at about 9 and about 14 MeV, respectively, but with some variation between ^{46}Ti and ^{50}Ti for each potential. These differences are presumably due to the different radii for these optical potentials, which result in different angular momentum barriers and slightly different wavelengths needed for resonance.

The presence of a $g_{9/2}$ single-particle state at about 9 MeV (for neutrons) is intriguing in that this is approximately where the searches with the BG potential located an enhancement in the $l=3$ and 4 contributions to the (p,n) reaction. The excitation functions, however, do not show an obvious resonancelike behavior in this energy region, which contrasts with the situation for the Mo isotopes.

Another possible explanation for the differing energy dependence of the (p,n) cross sections of the five titanium isotopes is that subtle changes in form factor might occur among the titanium isotopes. To investigate this more fully, we calculated the proton elastic cross section for the BG potential at 20 MeV for ^{46}Ti. We then varied the imaginary diffuseness by $\sim 10\%$ in either direction and then attempted to fit the values calculated originally by varying the radius and strength of the imaginary potential. The radius changed about 2% and the strength about 5% in the course of the search. As can be seen from Fig. 4, good fits could be obtained with the two new geometries. Only elastic scattering measurements extending over a broad range of angles and with good absolute accuracy ($\lesssim 10\%$) would suffice to distinguish between the modified potentials and the original BG potential. It is likely that a global potential will have discrepancies of at least this size in treating isotopic sequences. Further, the reaction cross sections given by the modified potential differ from the original Becchetti-Greenlees potential results by only 5%.

These revised (imaginary) geometries were then used in a calculation of the charge-exchange cross section for ^{46}Ti

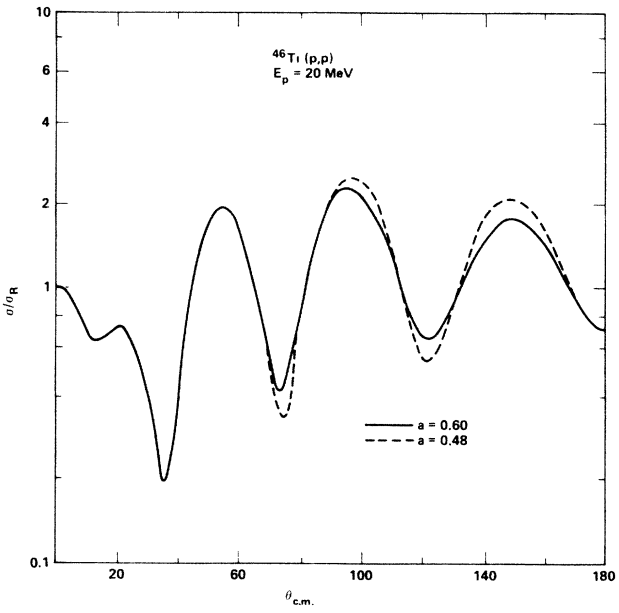

FIG. 4. Comparison of calculated elastic scattering cross sections for ^{46}Ti at 20 MeV. The diffuseness of the imaginary potential was both increased by 10% and decreased by 10% from the Becchetti-Greenlees value and the imaginary radius and strengths varied to achieve a best fit to the original Becchetti-Greenlees elastic scattering calculation.

in the energy region from 16 to 26 MeV. In each case the isovector strength was kept constant and equal to the BG value for both real and imaginary components. The imaginary isospin component was given the same geometry as the isoscalar imaginary potential. However, the change in diffuseness from 0.48 to 0.60 causes the (p,n) cross section to the ground-state analog to change from decreasing to increasing with bombarding energy from 16 to 26 MeV for an assumed constant isospin strength (see Fig. 5). Evidently, the cross section for charge exchange is rather sensitive to the form factor of the optical potential, the change in geometry causing the slope of the excitation function to change. Elastic scattering data over the energy range of the present data would be useful to determine whether the energy dependence of the cross sections for the various isotopes could be the result of subtle isotope-dependent differences in the optical potential form factors.

IV. COUPLED-CHANNEL CALCULATIONS

In this section we present the results of coupled-channel calculations for the Ti isotopes and compare with (p,n), (p,p), and (p,p') data. Our procedure is to couple the ground state, the 2_1^+ one-phonon state, the $0_2^+, 2_2^+, 4_1^+$, and all of their analogs (full coupling). The coupling form factors were taken from the collective model, and the deformation parameters β are taken from gamma decay lifetimes and inelastic scattering.

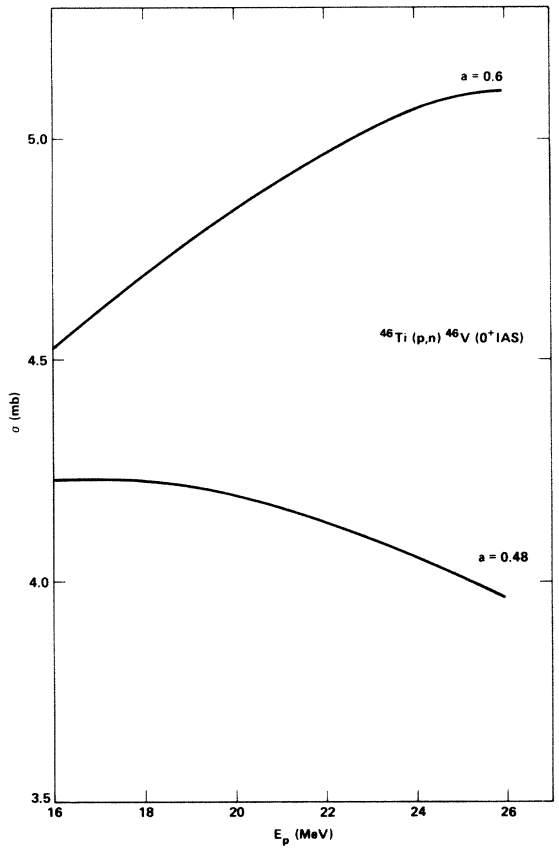

FIG. 5. ^{46}Ti(p,n) 0_1^+ analog integrated cross sections calculated with radii and diffuseness parameters adjusted upward and downward from the original Becchetti-Greenlees geometries (see the caption to Fig. 4).

A. Energy dependence

It was shown in Sec. III that the 0_1^+ analog cross sections have a rather rapid energy dependence. For example, ^{46}Ti varies from 6.2 mb at 11.5 MeV to 1.35 at 26 MeV. Coupling of low-lying collective states and their analogs has not been able to explain the energy dependence in other sets of isotopes.[9–11] It is still worthwhile, however, to make coupled-channel calculations as a function of energy to see just what can be explained by the model and what cannot. We have chosen to make the calculation for ^{48}Ti at the energies 15.3, 22.0, and 26.0 MeV of the (p,n) experiment, because for this nucleus there exist complementary elastic and inelastic proton data at 14.4, 16.5, 22.0, and 24.0 MeV.

Optical potentials used in these calculations were based on the set obtained from the BG potentials.[13] As described in Sec. II, proton potentials were held fixed and the Lane isospin strengths V_1 and W_1 were determined from a search (see Sec. III) on the 0_1^+ analog cross section using the Lane equations at the 22 MeV energy. The final potentials for protons and neutrons, respectively, are

$$V = 55.64 - 0.32E \pm V_1\xi + 0.4Z/A^{1/3}G \ , \tag{1}$$

$$W_V = 0.22E - 2.7 \text{ (or zero if negative)} \ , \tag{2}$$

$$W_s = 11.34 - 0.25E \pm W_1\xi \ , \tag{3}$$

where $V_1 = (30.5)/4$ and $W_1 = (66.6)/4$ MeV and

$$\xi = \frac{N-Z}{A} \ , \tag{4}$$

$$G = 1 \text{ (protons)} \ ,$$

$$= 0 \text{ (neutrons)} \ , \tag{5}$$

$$E = E_p \text{ (protons)} \ , \tag{6a}$$

$$E = E_p - E_C = E_p - 1.44\frac{\langle Z \rangle}{A^{1/3}} \text{ (neutrons)} \ . \tag{6b}$$

The optical potentials, which incorporate a single V_1/W_1 ratio averaged over isotopes and obtained from a two-channel Lane-model fit to the 22 MeV data, were used at all energies. The strengths Eqs. (1)–(3) have been adjusted to reproduce the BG proton best fit to the data on the average over the isotopes using the best-fit proton geometry and spin-orbit potential. This could have been done precisely isotope by isotope, but we prefer a global potential. The neutron potential that is appropriate for the analog channels is obtained by using the (p,n) fit, the best fit BG proton potential,[13] and Eqs. (1)–(6). No adjustment in the geometrical parameters was made.

Absorptive potentials were scaled down by a factor of 0.9 to correct approximately for the absorption included explicitly by the inelastic channel coupling. This factor is determined by comparing coupled-channel calculations with DWBA. The Lane terms, V_1 and W_1, in the coupling needed to be scaled from the pure Lane-equation values by factors of 1.7, 1.2, and 1.1 at 15.3, 22, and 26 MeV, respectively, to fit the measured 0_1^+ analog-state

TABLE II. Deformation parameter β used in coupled-channel calculations.

Transition	Probe	Mass 46	48	50
$0_1^+ \rightarrow 2_1^+$	em	0.309[a]	0.251[a]	0.166[a]
	(p,p')	0.261[b]	0.240[c]	0.149[b]
	(n,n')	0.298[e]	0.249	0.162
	(p,n')	−0.583[e]	0.133	0.045
$2_1^+ \rightarrow 4_1^+$	em		0.197[d]	
	(p,p')	0.261[f]	0.190[c]	0.149
	(n,n')	0.298	0.194	0.162
	(p,n')	−0.583	0.136	0.045
$2_1^+ \rightarrow 2_2^+$	em		0.167[d]	
	(p,p')	0.261	0.140[c]	0.149
	(n,n')	0.298	0.157	0.162
	(p,n')	−0.583	−0.067	0.045
$2_1^+ \rightarrow 0_2^+$	(p,p')	0.261	0.190[c]	0.149
	(n,n')	0.298	0.190	0.162
	(p,n')	−0.583	0.190	0.045
$0_1^+ \rightarrow 2_2^+$	(p,p')		0.05[c]	
$0_1^+ \rightarrow 4_1^+$	(p,p')		0.04[c]	
$0_1^+ \rightarrow 0_2^+$	(p,p')		−0.02[c]	

[a] $B(E2)$ from Ref. 20 using a Fermi distribution to calculate β_{em}.
[b] H. F. Lutz *et al.*, Phys. Rev. **187**, 1479 (1969). $\beta_{pp'}$ adjusted to data (first peak) using optical potentials of Eqs. (1)–(6).
[c] H. F. Lutz, Ref. 16.
[d] Reference 19.
[e] All $\beta_{nn'}$ and β_1 are calculated from $\beta_{pp'}$ and β_{em} using Eqs. (7) and (8).
[f] For ^{46}Ti and ^{50}Ti we had β_{em} and $\beta_{pp'}$ for the $0_1^+ \rightarrow 2_1^+$ only from which we calculated $\beta_{nn'}$ and β_{em} using our formulas. This same set was used throughout for all other transitions.

cross sections. The necessity for these scaling factors, which represents a cross section variation as large as $(1.7/1.1)^2 = 2.4$, demonstrates, as expected, that the coupling of low excited states and their analogs does not account for the rapid energy dependence of the analog cross section.

The coupling matrix elements are taken from the vibrational model except that the strengths for different transitions are taken from experiment. The values used are shown in Table II and will be discussed in more detail in Sec. IV B.

The (p,p) elastic scattering comparisons are shown in Fig. 6. The fits to the data[16] are satisfactory at 26 and 22 MeV (at which V_1 and W_1 were obtained from the two-channel fit), and the fit at 15.3 MeV represents adequately the average of the 14.4 and 16.5 MeV data. The considerable energy dependence of the angular distributions is also well followed by the coupled-channel calculations.

The inelastic (p,p') cross sections[17] are shown in Figs. 7–10. For the 2_1^+ excitation (Fig. 7) rather fine details of the angular distribution are reproduced by the coupled-channels calculations. The agreement is particularly striking at 22 MeV where (p,p') and (p,n) data are available at the same bombarding energy. Furthermore, the changing character of the 2_1^+ differential cross section at the other energies is followed by the calculations. Although the 4_1^+ data (Fig. 8) show more structure than the calculations, the magnitude and general slope are in agreement. The data for the 2_2^+ state (Fig. 9) is changing rapidly; the calculations at 15.3 agree fairly well with the data at 14.4 MeV but not at 16.5. The data and calculations agree fairly well at 22 and 26 MeV (data at 24 MeV) even though the character of the angular distributions has changed. The calculated results for the 0_2^+ state (Fig. 10) are about the right magnitude but at all three energies have much more structure than the experimental angular distributions. This state presumably has a very different character than the two-phonon structure, assumed in the calculation.

The calculations for the (p,n) 0_1^+ analog transition, which is known to be affected by channel coupling,[9,10,11,18] give the right slope and shape of the angular distributions, but as seen in Fig. 11 the maxima and minima are out of phase at middle angles. The substantial change in shape between 15.3 and 26 MeV is followed by the calculated curves, although the agreement at forward

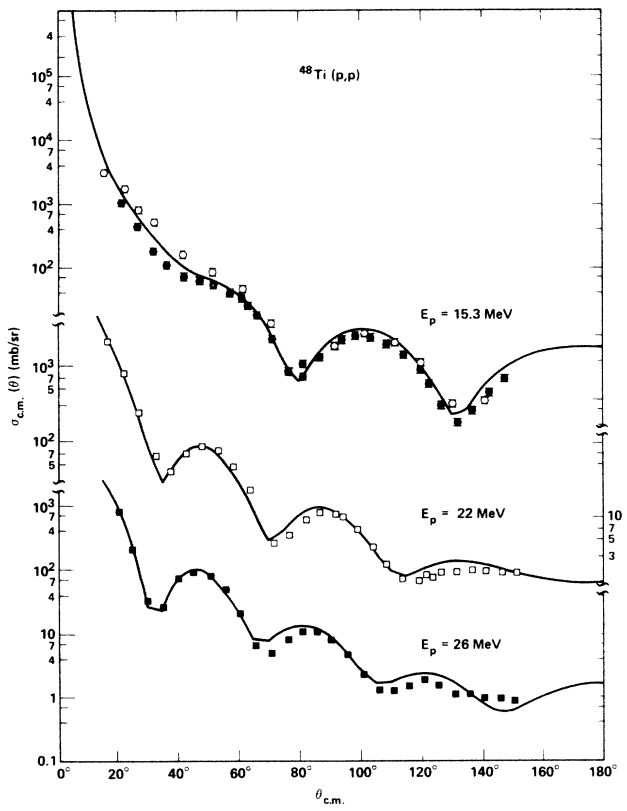

FIG. 6. ^{48}Ti(p,p) calculation at 15.3 MeV compared to data at 14.4 MeV (open circles) and at 16.5 MeV (closed circles), at 22 MeV compared to data at the same energy, and at 26 MeV compared to data at 24 MeV. Calculations involve full coupling with the standard Lane potentials and deformation parameters from Table II.

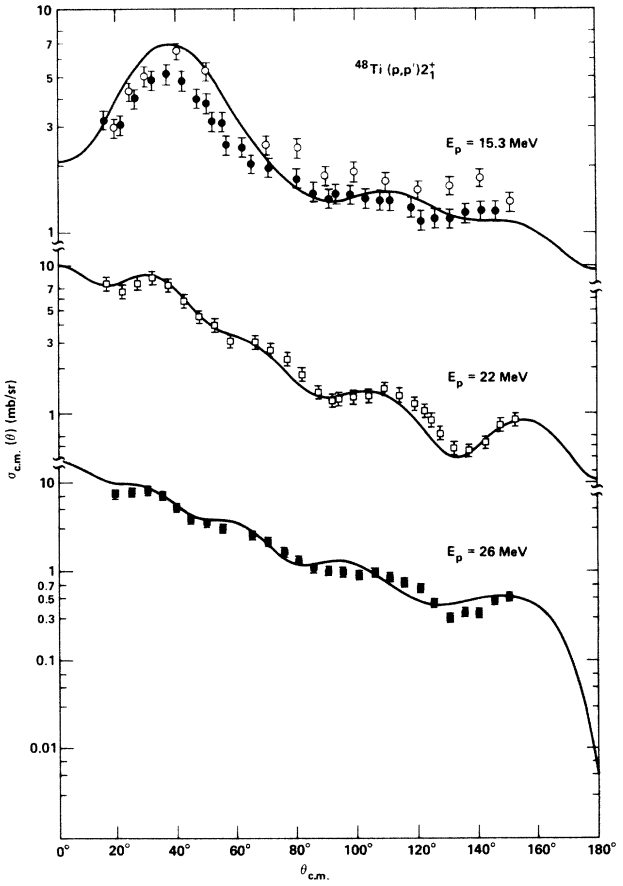

FIG. 7. ^{48}Ti(p,p') to the 2_1^+ state at 0.983 MeV. Otherwise the caption of Fig. 6 applies.

angles deteriorates at 26 MeV. The good agreement at 15.3 and 22 MeV in the forward peak came about from the use of the isospin potentials obtained from the search described in Sec. III and from the inclusion of channel coupling (see Sec. IV B and Fig. 13).

Also shown in Fig. 11 for comparison is a calculation using the BG isospin potential for ^{48}Ti, which completely misses the character of the angular distribution. The V_1 and W_1 parameters obtained from the search satisfy $W_1 > V_1$ compared to the BG values where $V_1 = 2W_1$. In both cases W_1 is purely surface and V_1 is purely volume. In order to see whether the improvement in $d\sigma/d\Omega$ from BG is due to the relative magnitudes of real and imaginary parts of the potential or to the greater degree of surface interaction in our V_1 and W_1, we have also calculated the differential cross section for ^{48}Ti at 15.3 MeV using purely surface real and surface imaginary Lane potentials with strengths 5.67 and 14.8 MeV, respectively. The resulting angular distribution, shown in Fig. 11, represents a significant improvement in phase of the second maximum while preserving the goodness of fit of the forward maximum. This is an indication of a preference for some degree of surface-real isospin potential.

The 2_1^+ excited analog-state differential cross sections

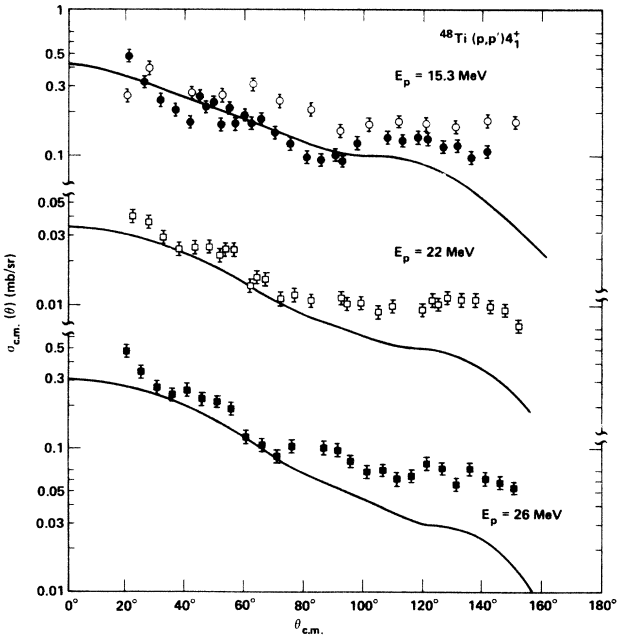

FIG. 8. ^{48}Ti(p,p') to the 4_1^+ state at 2.30 MeV. Otherwise the caption of Fig. 6 applies.

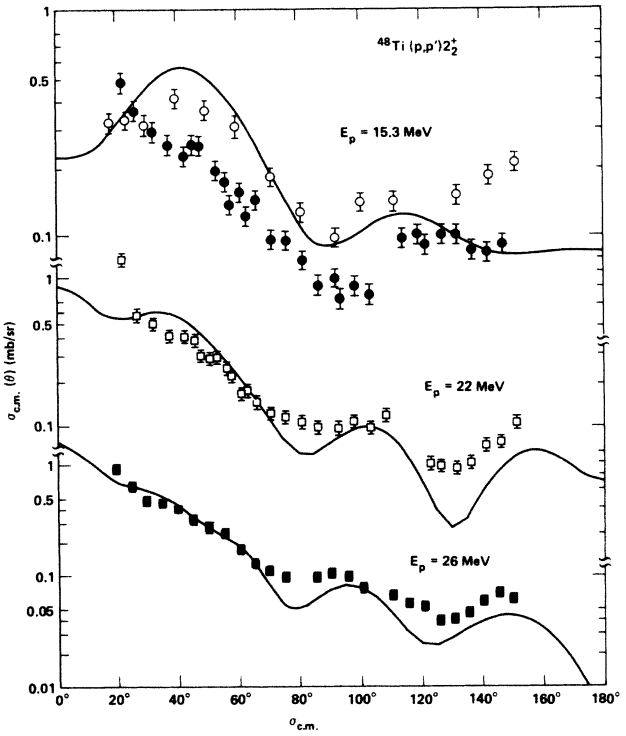

FIG. 9. ^{48}Ti(p,p') to the 2_2^+ state at 2.425 MeV. Otherwise the caption of Fig. 6 applies.

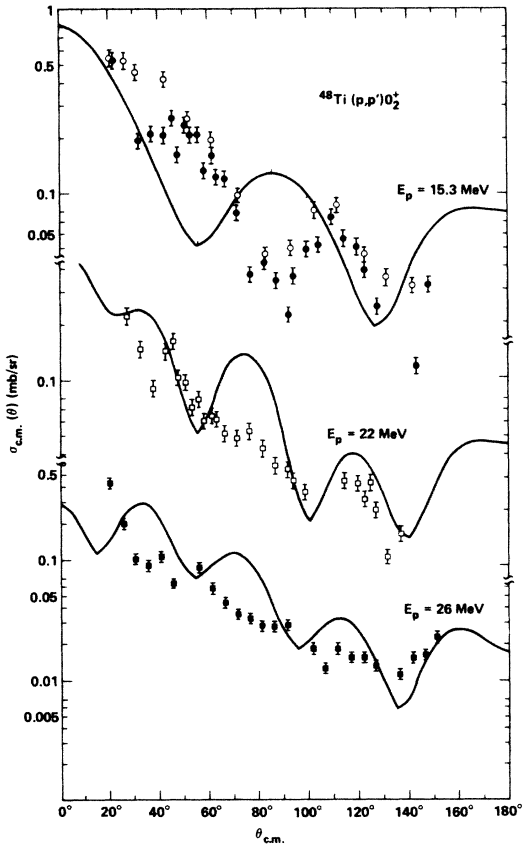

FIG. 10. ^{48}Ti(p,p') to the 0_2^+ state at 3.004 MeV. Otherwise the caption of Fig. 6 applies.

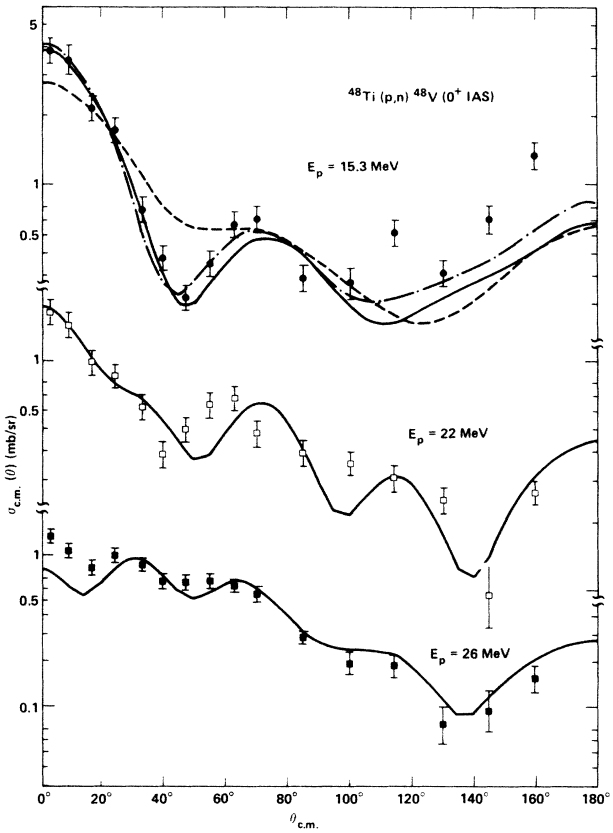

FIG. 11. ^{48}Ti(p,n) to the 0_1^+ analog state, calculations and data compared at three energies are compared. In the calculations the solid curve is the standard calculation using volume real and surface imaginary Lane charge-exchange interaction parameters, obtained from a search (see the text); the dot-dashed curve uses a surface real and imaginary forms, and the dashed curve uses the standard Becchetti-Greenlees ratio of 2 to 1 for volume real to surface imaginary Lane potential strengths.

are shown in Fig. 12. Again the slope and overall character of the angular distributions are followed by the calculated curves. It is interesting that the energy dependent normalization of V_1 required to fit the 0_1^+ analog is also appropriate for the 2_1^+ excited-analog excitations.

B. Isospin dependence

As mentioned in Sec. III, it has been shown previously that the $N-Z$ dependence of the (p,n) analog cross section, expected from the Lane model, breaks down when there is a strong variation in the collectivity of the excited 2_1^+ inelastic transitions among the even-even members of an isotopic chain. This effect has been seen[7,9–11] in Mo, Sm, and Se, the first two of which have the 2^+ deformation parameter β increasing with mass number A and the last of which has β decreasing with A. It was shown[9,18] that the coupling to the 2_1^+ inelastic and 2_1^+ analog channels provides three three-step routes, $0_1^+ \rightarrow 2_1^+ \rightarrow 0_1^+ \rightarrow 0_1^+$

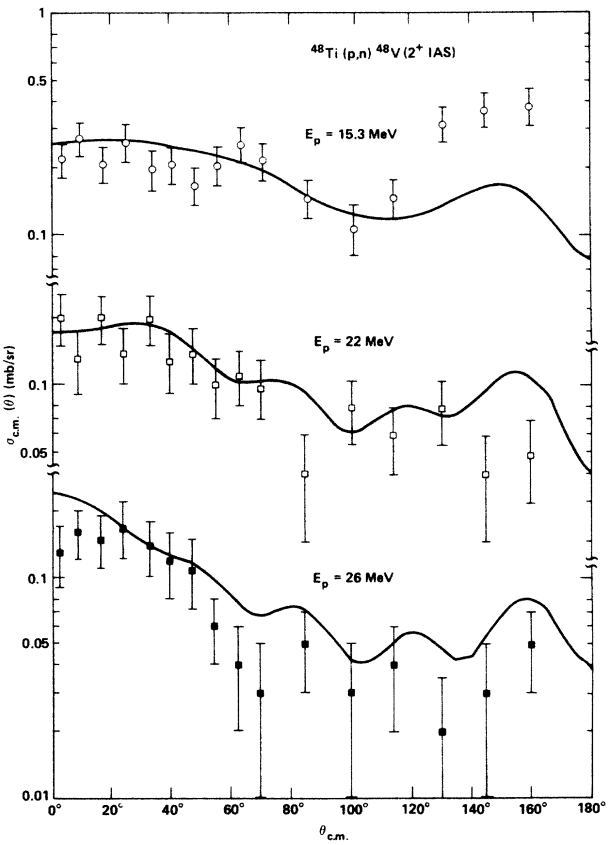

FIG. 12. ^{48}Ti(p,n) to the 2_1^+ analog state. The solid curves are the calculations using the ratios of volume real and surface imaginary obtained from the search of Sec. III (see the text).

analog, $0_1^+ \rightarrow 0_1^+$ analog$\rightarrow 2_1^+$ analog$\rightarrow 0_1^+$ analog, and $0_1^+ \rightarrow 2_1^+ \rightarrow 2_1^+$ analog$\rightarrow 0_1^+$ analog, all of which are approximately in phase with each other and out of phase with the dominant one-step $0_1^+ \rightarrow 0_1^+$ charge-exchange amplitude. Because of the large coupling strengths involved, these three-step mechanisms have larger amplitudes than various two-step processes such as $0_1^+ \rightarrow 2_1^+ \rightarrow 0_1^+$ analog. Their destructive interference with the dominant one-step charge-exchange mechanism causes the ratio $\sigma/(N-Z)$ to fall off with increasing deformation parameter, instead of being nearly constant, as the DWBA with the Lane potential would give.

Because the deformation parameter is decreasing with A among the Ti isotopes, channel-coupling effects are expected to be important in determining the differences in charge-exchange cross sections. We choose to make our comparison at 22 MeV, above the region of rapid energy dependence and at an energy for which proton elastic and inelastic scattering are available.

It has been demonstrated[19] over the past several years that the deformation parameter β is, in principle, dependent on the probe. This effect is most noticeable in single-closed-shell nuclei, in which quadrupole vibrations of nucleons of the type involved in the shell closure are partially "frozen in" by the shell gap and therefore have a smaller vibrational deformation parameter than the valence type of nucleons. The probe dependence results from these differences in vibrational amplitudes plus the fact that probes vary in the relative strength of their interaction with neutrons and protons. Electric multipole operators, for example, interact only with the nuclear protons, whereas the (α,α') probe interacts equally with neutrons and protons. Since in charge-exchange several channels are to be coupled involving different projectiles, consistency requires that the appropriate deformation parameter be used for each type of coupling.

The fact that the deformation parameters β_n and β_p for nuclear neutrons and protons are different can also be expressed in terms of isoscalar and isovector deformation parameters,

$$\beta_0 = \frac{N\beta_n + Z\beta_p}{A} , \tag{7a}$$

$$\beta_1 = \frac{N\beta_n - Z\beta_p}{N-Z} , \tag{7b}$$

which are equal only if $\beta_n = \beta_p$. In the collective model the appropriate deformation parameter for the $0_1^+ \rightarrow 2_1^+$ analog coupling should be β_1. According to the arguments presented above, for a single-closed-shell nucleus with valence protons such as ^{90}Zr, not only should $\beta_1 \neq \beta_0$ but β_1 may be negative. Interference between two-step and the one-step inelastic charge-exchange amplitudes should show the effects of the sign of β_1. Based on our earlier work, however, the effects may not be large because of the relative smallness and the near incoherence of the two-step amplitudes with the one- and three-step amplitudes.

Table II shows a list of deformation parameters for Ti obtained by Lutz *et al.*[17] from (p,p') and electromagnetic values from Bardin *et al.*[20] and from Christy and Häusser[21] as well as the β_0 and β_1 values calculated from them. For this calculation the formulas

$$\beta_{em} = \beta_p , \tag{8a}$$

$$\beta_{pp'} = \frac{NV_{pn}\beta_n + ZV_{pp}\beta_p}{NV_{pn} + ZV_{pp}} , \tag{8b}$$

$$\beta_{nn'} = \frac{NV_{nn}\beta_n + ZV_{np}\beta_p}{NV_{nn} + ZV_{np}} , \tag{8c}$$

are used with $V_{np}/V_{nn} = 3$, consistent with the Lane model.

The trend of the experimentally determined β_{em} or $\beta_{pp'}$ as a function of isotope satisfies our expectations on the basis of an $f_{7/2}$ shell description of Ti; i.e., there is a steady decrease in β with increasing A until the neutrons fill the $f_{7/2}$ shell at ^{50}Ti. However, the differences between β_{em} and $\beta_{pp'}$ do not satisfy our expectations. Like ^{90}Zr, the nucleus ^{50}Ti is closed on neutrons and should therefore satisfy the inequality $\beta_{pp'} \approx \beta_n < \beta_p = \beta_{em}$, and, furthermore, from Eq. (7b) β_1 should be small or negative. For ^{46}Ti, there are two $f_{7/2}$-shell protons and four $f_{7/2}$-shell neutrons. There should therefore be more $0\hbar\omega$ strength for neutrons than protons, which leads us to expect $\beta_n > \beta_p$, which in turn implies through Eq. (8) that $\beta_{pp'} > \beta_{nn'}$, opposite to that shown in Table II.

On the other hand Lawson[22] has shown that the 0_2^+

state in ^{48}Ti has significant $(\pi d_{3/2})^2(\pi f_{7/2})^4(\nu f_{7/2})^{-2}$ configurations. The presence of $(\pi d_{3/2})^2(\pi f_{7/2})^4$ configurations, which is also likely in other states and other Ti isotopes, would considerably enhance proton transition strengths. Configurations involving one or more neutrons in the $f_{5/2}$, $p_{3/2}$ shells probably also contribute significantly to neutron transition strength. Whether neutrons or protons win out in transition strength is a question which must be answered experimentally. Having taken $\beta_{pp'}$ and β_{em} from experiment, we now examine whether the (p,n) reaction can confirm the inequality.

Figure 13 shows the experimental data for the 22 MeV ^{46}Ti(p,n) 0_1^+ analog transition. Calculated results are shown for analog coupling only, for full coupling with uniform β parameters, $\beta_{pp'}=\beta_{nn'}=\beta_0=\beta_1$, for full coupling with the β parameters of Table II, and for two-step only (β values from Table II with the direct $0_1^+\rightarrow 2_1^+$ analog couplings omitted). Although the phasing of the calculated differential cross sections misses the experimental phase, the calculation with full coupling using empirical β values is by far the best, particularly at forward angles.

Figure 14 shows the data for the 2_1^+ excited analog transition at 22 MeV with the calculated curves for ^{46}Ti for full coupling with uniform and with empirical β's. Also shown is the result of the two-step calculation. Surprisingly, only the full coupling calculation with the β parameters from Table II comes close to the data. It is also remarkable that the calculation with uniform β parameters but full coupling is weaker than the one leaving out the direct $0_1^+\rightarrow 2_1^+$ analog coupling. This is due to the usual[18] destructive interference when β_1 is positive. In Table III are listed the integrated cross sections for these

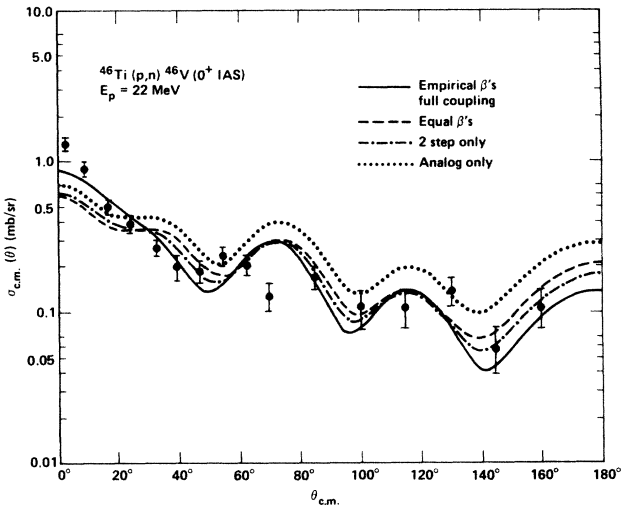

FIG. 13. ^{46}Ti(p,n) to the 0_1^+ analog state. All calculated curves use the standard Lane parameters. The solid curve is calculated with the β values of Table II. The dashed curve results from the use of uniform β values (same in all couplings); the dot-dashed curve results from a calculation like that of the solid curve but with the direct $0_1^+\rightarrow 2_1^+$ analog and 0_1^+ analog to 2_1^+ inelastic charge-exchange couplings left out. The dotted curve results from a pure Lane-Model calculation; that is, only the 0_1^+ ground state and the 0_1^+ analog are coupled.

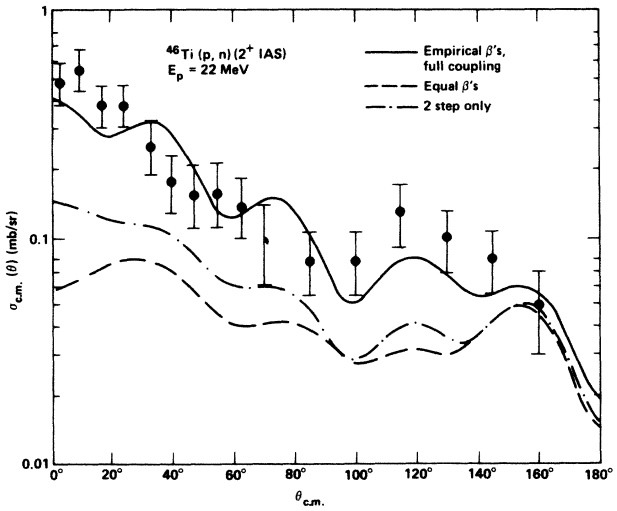

FIG. 14. ^{46}Ti(p,n) to the 2_1^+ analog. Calculated curves are as in Fig. 12.

three cases plus a DWBA equivalent calculation in ^{46}Ti (only $0_1^+\rightarrow 2_1^+$ analog in weak coupling) using coupling determined from the β parameters of Table II.

As mentioned above, in our earlier work on (p,n) to excited analog states[8-11] it was found that the one- and two-step amplitudes are close to 90° out of phase. If the amplitudes were exactly 90° out of phase, the one- and two-step cross sections would approximately add, giving us something between the numbers of the third and fourth lines of Table III. As pointed out in Ref. 18 for positive β_1 values, what interference there is between one- and two-step mechanisms is destructive, as we see in Table III, third line. Correspondingly for negative values of β_1, it is constructive, as we see from Table III, fourth line.

Ignoring all the two-phonon couplings and defining amplitudes A_1 and A_2 for the one- and two-step mechanisms for unit β values as

$$|A_2| = \left|\frac{\sqrt{\sigma_{\text{two step}}}}{\bar{\beta}_{in}}\right|, \quad |A_1| = \left|\frac{\sqrt{\sigma_{\text{one step}}}}{\beta_1}\right|, \qquad (9)$$

where $\bar{\beta}_{in}=(\beta_{pp'}+\beta_{nn'})/2$, we may calculate crudely the

TABLE III. Interference effects in channel coupling in ^{46}Ti(p,n) at energy 22 MeV.

Calculation	β_1/β_0[e]	β_n/β_p[e]	σ	σ[d]
One-step only[a]			0.556 mb	
Two-step only[b]			0.709 mb	
Full coupling[c]	1	1	0.544 mb	0.578
Full coupling[a]	−2	1.2	1.556 mb	1.63

[a]Parameters of Table II.
[b]Uniform β parameters except for $0_1^+\rightarrow 2_1^+$ analog and $2_1^+\rightarrow 0_1^+$ analog.
[c]Uniform β parameters.
[d]Calculated from Eq. (10) using a phase angle of 107°.
[e]$0_1^+\rightarrow 2_1^+$ transition.

total cross section including both one- and two-step couplings as

$$\sigma = |\beta_1 | A_1 | + \bar{\beta}_{in} | A_2 | e^{i\phi} |^2 , \quad (10)$$

where ϕ is the phase angle of A_2 with respect to A_1. For the two cases of the third and fourth lines of Table III, Eq. (10) gives cross sections shown in the fourth column of the table for a choice of phase angle of 107°, in reasonable agreement with the results of the full coupling calculations.

From our previous experience with phases of multistep processes[9,18] we would expect A_2, which requires one propagator and one inelastic scattering more than A_1, to have an extra phase of $(-i)$ for the open-channel propagator times the phase $(V+iW)$ for the extra inelastic interaction. Choosing the effective ratio of W/V to be between the extreme limits of 0.2 and 0.5 gives an overall phase of between 101° and 112°, in good agreement with the choice of 107° used above. It seems therefore that we understand roughly the phases of the interfering amplitudes.

Figures 12 and 15 show that for ^{48}Ti and ^{50}Ti, which have positive and near zero values of β_1, respectively, the magnitude of the 2_1^+ analog cross section is also fit by the coupled-channel calculation. It is significant that both of these nuclei have considerably smaller cross sections than ^{46}Ti, even though both have larger neutron excesses and even though ^{48}Ti has a deformation parameter β nearly equal to that of ^{46}Ti. The constructive interference of one- and two-step amplitudes and the rather large value of β_1 for ^{46}Ti make a very large enhancement in the 2_1^+ analog cross section, which is required to fit the data.

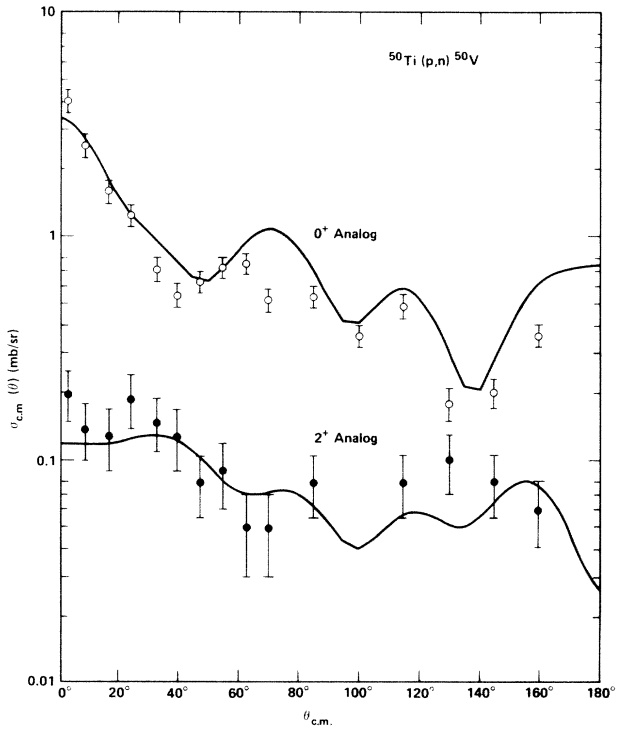

FIG. 15. 22 MeV ^{50}Ti(p,n) to the 0_1^+ and 2_1^+ analog states. The calculations use standard Lane potential parameters and full coupling with the deformation parameters of Table II.

V. SUMMARY AND DISCUSSION

We have presented measurements of the differential cross section for the excitation of analog states in the Ti isotopes at several low bombarding energies. As in previous studies[7-11] of isotopic chains, the 0_1^+ analog cross sections are not proportional to $(N-Z)$ but have a strong dependence on isotope, which is correlated with collectivity. In addition, a strong energy dependence within several MeV of threshold, similar to that found in Mo, Sm, and Se isotopes, is also found in Ti. The data have been analyzed within both the simple Lane model and a model including inelastic and analog couplings.

A significant sensitivity of the (p,n) excitation function for populating the ground-state analog to the details of the imaginary (surface) isovector potential strength was observed by changing the imaginary radius slightly and compensating with modifications in the diffuseness. The elastic differential cross section could be maintained almost invariant, while the slope as a function of energy of the (p,n) excitation function changed from positive to negative. Obviously, studies of (p,n), (p,p), and (n,n) reactions on the same nucleus over a range of energies are needed to pin down form factors and isovector strengths. At present we assume that the real and imaginary isovector strengths have the same form factors as their isoscalar counterparts, but it would be desirable to have a large enough data set to test this assumption.

Good fits to the 0_1^+ analog differential cross sections are obtained only with inclusion of channel coupling and with V_1 and W_1 parameters obtained from the Lane model by searching on the (p,n) 0_1^+ data. It is not clear whether the searched values of V_1 and W_1 are superior because of the larger imaginary to real strength or because of a greater degree of surface interaction. In DWBA the complex phase of the interaction is irrelevant; only the radial form factor is important. When channel coupling is included, the phase can make a difference. In a test calculation on ^{46}Ti, an improved angular distribution was obtained when some real surface strength was included in the Lane potential. This result is suggestive, but does not constitute sufficient evidence that a surface real isospin potential is required.

In the Ti analog (p,n) reaction, inelastic channel-coupling effects are again important. As in our other studies[7,9-11] they dominate the 2_1^+ analog excitation, strongly affect the 0_1^+ analog, and account for differences in the $N-Z$ dependence of cross sections among members of an isotopic chain. Although our present measurements do not reproduce the data of Ref. 8 exactly, we do obtain $\sigma/(N-Z)$ approximately constant for the even isotopes at energies of about 15.3 MeV. We note, however, that this result is not very significant because the cross section ratios are so strongly energy dependent in this region.

It was found in our analysis of 2_1^+ analog cross sections that it was absolutely necessary to take into account the

known differences between neutron and proton deformation parameters. This is not very important for the inelastic couplings since the 0_1^+(p,p') 2_1^+ and 0_1^+ analog (n,n') 2_1^+ analog couplings, which enter the $0_1^+ \rightarrow 2_1^+$ analog excitation amplitude symmetrically, compensate each other. It is, however, very important for the $0_1^+ \rightarrow 2_1^+$ charge-exchange coupling. In ^{46}Ti the empirical β_n and β_p values with $\beta_p > \beta_n$ imply a negative β_1. In such a case, the interference between the dominant two-step mechanisms $0_1^+ \rightarrow 2_1^+ \rightarrow 2_1^+$ analog and $0_1^+ \rightarrow 0_1^+$ analog $\rightarrow 2_1^+$ analog and the weaker direct mechanism $0_1^+ \rightarrow 2_1^+$ analog, although mostly incoherent, have constructive phases. In ^{46}Ti it makes about a factor of 3 difference in cross section when the sign of β_1 is changed (see Table III and Fig. 15). The empirical negative sign agrees with experiment. The experimental differential cross sections for all three even isotopes are also consistent with the very different empirical values of β_1 (see Table II) for both the 0_1^+ and 2_1^+ analogs. The differential cross sections for both at small angles exhibit rather different behavior for ^{46}Ti, which has a large negative β_1, and ^{48,50}Ti, which have smaller positive β_1. These differences in the data are also present in the coupled-channel calculations.

In most of our previous work on channel-coupling effects in charge exchange,[7,9–11,18] the one-step $0_1^+ \rightarrow 2_1^+$ analog coupling has not played a very large role in excitation of the 2_1^+ analog state, which goes primarily by two-step inelastic scattering followed by charge exchange or vice versa. The one exception[18] was ^{26}Mg(p,n). In that case as in ^{46}Ti the smallness of the nuclei and therefore the inelastic excitation part of the two-step mechanism and the rather large value and negative sign of β_1 combine to make the one-step amplitude much more important than in the other cases we have dealt with.

The coupling to low-lying inelastic states does not explain the energy dependence of the 0_1^+ analog state. Nevertheless, the use of an energy dependent interaction obtained from normalizing to the 0_1^+ analog integrated cross section seems to be adequate for accounting for energy dependences in the angular distribution of 0_1^+ states and for the experimental strength of the excited 2_1^+ analog transitions. These significant facts should be taken into account in consideration of possible mechanisms for explaining the energy dependence. The mechanism must be one which affects all analog transitions $J^\pi \rightarrow J^\pi$ analog in the same way in order to behave like an energy-dependent renormalization of the charge-exchange interaction.

Note added in proof. A recent coupled-channels analysis of ^{54,56}Fe simlar to that for Ti has been carried out by Smith *et al.*, Phys. Rev. C 33, 847 (1986). The β_1 differences which are determined empirically, comparing (n,n') and (p,p') and which are in agreement with an RPA calculation, also account remarkably well for the differences in (p,n')2_1^+ cross sections for the two isotopes.

ACKNOWLEDGMENTS

The other authors wish to express their feelings of loss of friend and colleague, Cal Wong, who died suddenly during the final stages of completion of this work. He had been actively involved in the preparation at the time of his death. The work reported in this paper was done under the auspices of the U.S. Department of Energy under Contracts No. W-7405-ENG-48 at Lawrence Livermore National Laboratory and No. DE-AT06-79ER 10405 at Oregon State University and No. DE-AC02-76ER 02490 at Ohio University.

[1]A. M. Lane, Phys. Rev. Lett. **8**, 171 (1962); Nucl. Phys. **3**, 676 (1962).
[2]P. S. Miller and G. T. Garvey, Nucl. Phys. **A163**, 65 (1971).
[3]G. W. Hoffmann, W. H. Dunlop, G. J. Igo, J. G. Kulleck, J. W. Sunior, and C. A. Whitten, Jr., Nucl. Phys. **A187**, 577 (1972).
[4]G. W. Hoffmann, W. H. Dunlop, G. J. Igo, J. G. Kulleck, C. A. Whitten, Jr., and W. R. Coker, Phys. Lett. **40B**, 453 (1972).
[5]C. Wong, J. D. Anderson, J. W. McClure, B. A. Pohl, and J. J. Wesolowski, Phys. Rev. C **5**, 158 (1972).
[6]C. Wong, J. D. Anderson, J. C. Davis, and S. M. Grimes, Phys. Rev. C **7**, 1895 (1973).
[7]S. M. Grimes, C. H. Poppe, J. D. Anderson, J. C. Davis, W. H. Dunlop, and C. Wong, Phys. Rev. C **11**, 158 (1975).
[8]C. D. Goodman, J. D. Anderson, and C. Wong, Phys. Rev. **156**, 1249 (1967).
[9]V. A. Madsen, V. R. Brown, S. M. Grimes, C. H. Poppe, J. D. Anderson, J. C. Davis, and C. Wong, Phys. Rev. C **13**, 548 (1976).
[10]C. Wong, V. R. Brown, V. A. Madsen, and S. M. Grimes, Phys. Rev. C **20**, 59 (1979).
[11]C. Wong, S. M. Grimes, C. H. Poppe, V. R. Brown, and V. A. Madsen, Phys. Rev. C **26**, 889 (1982).
[12]The 24 MeV data set was incomplete and was not used in the later comparisons with theory.
[13]F. D. Becchetti and G. W. Greenlees, Phys. Rev. **182**, 1190 (1969).
[14]L. Rosen, J. G. Beery, A. S. Goldhaber, and E. H. Auerbach, Ann. Phys. (N.Y.) **34**, 96 (1965).
[15]D. M. Patterson, R. R. Doering, and Aaron Galonsky, Nucl. Phys. **A263**, 261 (1976).
[16]D. Wilmore and P. E. Hodgson, Nucl. Phys. **55**, 673 (1964).
[17]H. F. Lutz, D. W. Heikkinen, W. Bartolini, and I. D. Proctor, Nucl. Phys. **A231**, 365 (1974).
[18]V. A. Madsen and V. R. Brown, in *The (p,n) Reaction and the Nucleon-Nucleon Force*, edited by C. D. Goodman *et al.* (Plenum, New York, 1980).
[19]A. M. Bernstein, V. R. Brown, and V. A. Madsen, Comments Nucl. Part. Phys. **11**, 203 (1983).
[20]T. T. Bardin, J. A. Becker, and T. R. Fisher, Phys. Rev. C **7**, 190 (1972).
[21]R. F. Christy and O. F. Häusser, Nucl. Data Tables **11**, 281 (1972).
[22]R. Lawson, Nucl. Phys. **A173**, 17 (1971).